Submitted to J. Electrochem. Soc
3/25/97

Electrochemical Properties of $LaNi_{5-x}Ge_x$ Alloys in Ni-MH Batteries

C. Witham, A. **Hightower,** B. **Fultz**

Division of Engineering and Applied Science, California Institute of Technology,

Pasadena, California 91125

and

B. V. **Ratnakumar**[a], and R C. Bowman, **Jr.**[b]

[a] *Electrochemical Technologies Group*

[b] *Advanced Thermal and Structural Technology Group*

Jet Propulsion Laboratory, 4800 Oak Grove Dr., Pasadena, California 91109

ABSTRACT

Electrochemical studies were performed on $LaNi_{5-x}Ge_x$ metal hydride alloys with $O \leq x \leq 0.5$. We carried out single-electrode studies to understand the effects of the Ge substituent 011 the hydrogen absorption characteristics, the electrochemical capacity, and the electrochemical kinetics of hydrogen absorption and resorption. The electrochemical characteristics of the Ge-substituted alloys are compared to those of the Sri-substituted alloys reported earlier. $LaNi_{5-x}Ge_x$ alloys show compositional trends similar to $LaNi_{5-x}Sn_x$ alloys, but unlike the Sn substituted alloys, Ge-substituted alloys continue to have

facile kinetics for hydrogen absorption/desorption at high solute concentrations. Cycle lives of $LaNi_{5-x}Ge_x$ electrodes were measured in 300 mAh laboratory test cells and were found to be superior to the Sn-substituted $LaNi_5$ and comparable to a $Mm(Ni,Co,Mn,Al)_5$ alloy. The optimum Ge eontent for $LaNi_{5-x}Ge_x$ metal hydride alloys in alkaline rechargeable cells is in the range $0.4 < x \leq 0.5$.

INTRODUCTION

Alkaline rechargeable cells with nickel oxyhydroxide positive electrodes and inter-metallic hydride negative electrodes are being used widely in three portable electronics applications: camcorders, computers, and cellular phones, and are considered as a near-term technology for electric vehicles. Their high specific energy and energy density combined with environmental compatibility are motivating widespread use. Cost and cycle life, on the other hand, are deterrents, especially with the advent of Li ion rechargeable cells, and are topics of research at various laboratories.

Although multiphase "AB_2" alloys containing Laves phases are being actively pursued due to their inherent high hydrogen absorption capacity, the majority of commercial nickel metal-hydride (Ni-MH) cells utilize "AB_5" intermetallic alloys of rare earth and transition metals. The AB_5 alloys are multi-component, primarily Haucke phase materials and are derivatives of $LaNi_5$. Economic reasons prompted a replacement of La with Mm (misch metal), a naturally occurring mixture of lanthanides (La, Ce, Pr and Nd), in the current formulations such as $(Mm)(Ni\text{-}Co\text{-}Mn\text{-}Al)_5$.[1,2] The various substituents for La and Ni help alleviate problems of capacity degradation during electrochemical cycling. The systematic effects of these alloy modifications and the reasons for these effects are active topics of research.[3,4]

The most important result of alloy substitution for the extension of cycle life is thought to be a reduction in volume expansion upon hydride formation.[3,4] Cobalt substitution for Ni has been identified as one of the most effective solutes in this respect and results in a greatly reduced tendency towards fragmentation and corrosion[3,5] leading to batteries with long lifetimes. Unfortunately, cobalt is an expensive element and the specific role of Co is not well understood, The partial substitution of Sn for Ni has been found to significantly enhance stability during gas phase thermal cycling[6] and electrochemical cycling.[7] In addition to reducing the volume expansion upon hydriding,[8] Sn substitution also reduces plateau pressures and absorption- resorption hysteresis with only a small reduction in hydrogen storage capacity.[9] Willems[5] has speculated that Si and Al substitutions inhibit corrosion during electrochemical cycling through the formation of passivating oxide films on the surfaces. However, photoelectron spectroscopy studies[10,11] on cycled powder electrodes of both $LaNi_{5-x}Si_x$ and $LaNi_{5-x}Al_x$ did not indicate the presence of these solute-enriched surface oxide films. Lower volume expansion upon hydriding for the Al and Si substituted alloys were identified by Meli, et al.[10,11] as the source of increased corrosion resistance.

One problem associated with solute substitutions in AB_5 alloys is that it often reduces the maximum hydrogen storage capacity and the kinetics of hydrogen absorption and desorption.[4] 1 n our recent systematic studies[7] of various Sn-substituted alloys $LaNi_{5-x}Sn_x$ with $0.0 < x \leq 0.5$, wc observed improved capacity retention during electrochemical

cycling as the Sn content was increased, and reduced equilibrium hydrogen absorption pressure due to larger unit cell volume. On the other hand, the electrochemical kinetics[7] for the hydrogen absorption and resorption processes initially improve with Sn contents up to x = 0.3 but become sluggish at the higher Sn substitution levels, The optimum Sn concentration with respect to capacity, kinetics, and cycle life was found to be between x = 0.2 and x = 0.3.

In a more recent study[12], we have briefly reported similar beneficial effects with Ge substitutions for Ni in $LaNi_5$. The capacity retention during cycling is comparable to that achieved with Sn, although more Ge than Sn is required to achieve low absorption pressures. Encouraged by these preliminary results, we have carried out a detailed study of $LaNi_{5-x}Ge_x$ alloys with $0.1 \leq x \leq 0.5$. These studies are aimed at identifying the effect of the Ge additive on electrochemical characteristics of the metal hydride alloys, including the alloys' kinetics of charge transfer and diffusion during the hydriding process as well as their cyclic lifetimes in 300 mAh laboratory test cells.

EXPERIMENTAL

The $LaNi_{5-x}Ge_x$ alloys were prepared by induction-melting in an argon atmosphere. To insure a homogeneous distribution of Ge in the alloys, the ingots were subsequently annealed in evacuated quartz ampoules at 950°C for 72 hours. Each alloy

was activated by an initial hydrogen absorption and five subsequent thermally driven absorption/resorption cycles. During each resorption step the alloys were heated to -513 K and evacuated to 10^{-4} torr by a Tribodyn oil-free molecular drag vacuum pump. The chemical composition and homogeneity of the alloys were characterized by x-ray microprobe analysis, and the crystal structure was examined by X-ray diffractometry (XRD). Energy Dispersive X-ray Analysis was performed with a JEOL SuperProbe 733 electron microprobe. X-ray data were obtained with an INEL CI'S-120 powder diffractometer using Co $K\alpha$ radiation ($\lambda = 1.7902$ Å).

For the electrochemical measurements, the fine alloy powder ($<38\mu m$) was mixed with 19'% conductive diluent, i.e., 1 NCO 255 filamentary nickel powder (1pm), and 5°/0 Teflon binder. The anodes for the cycle life studies (area: 2.54 x 2.54 cm) were fabricated by hot-pressing the mixture at 300°C onto an expanded Ni screen. The anodes for the basic electrochemical studies were fabricated by filling BAS (Bio-Analytical Systems) disk electrodes with electrode powders of equal quantities to ensure consistent values for the electrode area (0.09 cm^2) and porosity. NiOOH electrodes from an aerospace Ni-Cd cell, supplied by Eagle-Picher, formed the counter electrode. A three-electrode flooded half-cell with a Luggin capillary for the Hg/HgO reference electrode was used for the basic electrochemical studies. For the cycle life studies, the same components were assembled in a prismatic glass cell, with Nylon (Pellon 2516) separator for electrical insulation and Teflon shims for required compaction. The electrolyte contained 31 w% KOH solution

prepared with twice-distilled low-conductivity water Electrochemical measurements (DC) were performed with an EG&G 273 Potentiostat/Galvanostat interfaced to an IBM-PC, using EG&G Corrosion Software 252. AC impedance measurements were carried out with the EG&G 273 Potentiostat and Solartron 1255 Frequency Response Analyzer, using EG&G Impedance software 388. Cycling of the 300 mAh, prismatic cells was carried out with an automatic battery cycler made by Arbin Corp., College Station, TX. The cycling conditions included discharging at a constant current of 150 mA/g (C/2 rate) to -0.5 V vs. Hg/HgO and charging at a constant current of 60 mA/g (C/5 rate) to a charge return of' 115°A to ensure complete charging of the metal hydride electrode.

RESULTS AND DISCUSSION

X-RAY DIFFRACTION

As described earlier[13], X-ray diffraction (XRD) patterns of $LaNi_{5-x}Ge_x$ alloys with different Ge contents confirmed that all alloy compositions except for $x = 0.5$ were single phase materials with the $CaCu_5$ crystal structure (Haucke phase). At the composition x = 0.5, weak XRD peaks from a second phase were observed. This result was confirmed by microprobe analysis, which revealed the presence of tiny equiaxed precipitates of approximately LaNiGe composition in the Haucke phase matrix of $LaNi_{4.5}Ge_{0.5}$. With increasing Ge content, the diffraction peaks shift to smaller angles. The shifted XRD

peak positions were used to obtain unit cell lattice parameters and volumes.[13] The enlargement of the unit cell upon substituting Ge for Ni is not so great as for Sn substitution, since the metallic radius of Ge (O. 1378 nm) is small compared to Sn (O. 1631 run)?

ISOTHERMS

To understand the hydrogen absorption characteristics of the $LaNi_{5-x}Ge_x$ alloys, pressure composition isotherms were generated both in the gas phase and in the electrochemical environment. 'I'he gas phase (*pcT*) isotherms of these alloys at various temperatures were discussed previously [13], but are compared to the present isotherms from electrochemical (EC) isotherm measurements in Fig. 1.

'he electrochemical isotherms presented in Fig. 1 were obtained in the same manner as for $LaNi_{5-x}Sn_x$ alloys.[7] EC isotherms were derived from the equilibrium electrode potentials at different stages of hydrogen absorption or desorption, [15] achieved by galvanostatic charge or discharge. In the figure, the measured potentials have been converted to the equivalent pressures by the Nernst equation. These experiments are similar to coulometric titrations.[16] One difference between the EC absorption isotherms and the gas-phase absorption isotherms is that there is a weaker inflection in the pressure at the end of the EC absorption isotherm, This inflection results from the increase in the equilibrium hydrogen pressure, but the pressures in our partial l y-scaled electrochemical

cells are limited to one atmosphere, The discharge isotherms should be more reliable, although the difficulty in charging alloys higher than 1 atm and polarization losses in the electrochemical cell will attenuate the maximum hydrogen capacity measured. As evident from Fig. 1, a good correlation was obtained between the gas-phase and electrochemical isotherms, as found in our earlier studies with Sri-substituted alloys.[7] The absorption and resorption plateau pressures and the hysteresis ratio decrease with increasing Ge content, 13 The exponential decrease[13] in plateau pressure with increasing unit cell volume is consistent with the observations of Gruen, et al.[17] This decrease in the plateau pressure with the solute content is smaller in Ge-substituted alloys than in Sn- substituted alloys as summarized in Fig. 2 of reference 13. This is consistent with the smaller increase in the unit cell volume upon Ge substitution.

In order to estimate the effect of kinetics on the realizable electrochemical capacity as a function of the Ge concentration, the mid-point discharge potentials are compared with the correpsonding thermodynamic (equilibrium) potentials calculated from the resorption isotherms in Fig. 2,. Also included in Fig. 2 are the equilibrium and discharge potentials from the Sn-substituted alloys. The equilibrium discharge potentials decrease with an increase in the solute concentration, as evident from a decrease in the plateau pressures. It is evident from the figure that the overpotentials tend to increase at high Sn contents, especially at compositions in excess of 0.3. *For the* Ge solute, however, the increase. in the overpotentials at high solute concentrations is not as large as with Sn,

implying that the kinetics of hydrogen absorption and resorption are unaffected at high Ge concentrations. Further detailed measurements on the kinetics of hydrogen absorption and resorption in $LaNi_{5-x}Ge_x$ alloys have been carried out to verify this assertion and are described below.

HYDROGEN A1ISORP'I'1ON CAPACITY

The hydrogen absorption capacities of the $LaNi_{5-x}Ge_x$ alloys were measured in the electrochemical cell and are compared to gas-phase capacities in Fig. 3. The slight decrease in the gas phase capacities with increasing Ge content results from the increase in formula weight (atomic weight of a single AB_5 unit) and probably the blocking of some hydrogen sites by the solute substitution.[3] The electrochemical capacity was taken to be the maximum capacity achieved during cycling of the prismatic cells,

Figure 3 shows that the maximum capacities of the Ge-substituted alloys as measured in partially sealed prismatic cells are slightly lower than the corresponding gas-phase capacities, as also seen in our previous work with $LaNi_{5-x}Sn_x$.[7] The capacity suppression at low solute contents is notable, and can be attributed to the high plateau (absorption) pressures of the anode materials, which prevents their complete utilization in our electrochemical test cells. The charge potential is higher for alloys with higher plateau pressures, and under these conditions the competing hydrogen evolution reaction is favored over hydrogen absorption by the metal hydride, and hydrogen gas is formed at

the electrode surface. At higher solute compositions, where plateau pressure is not a problem, the charge process becomes efficient and the difference between the electrochemical capacities and gas-phase capacities is approximately constant. We believe this residual discrepancy can be attributed to several sources. Our electrodes are hot pressed at 300°C in air. During this step a surface oxidation layer will be formed from active material, thus decreasing the material's maximum capacity. *[8] In addition, the stronger surface (hydroxide) films formed in the electrochemical environment may impose larger polarization losses, both in the charge transfer as well as the diffusion processes, especially at the high discharge rates and low electrode dispersion in our tests. The formation of such films is likely to be aided by the low discharge cut-off potentials. All the above factors can result in an incomplete utilization of the metal hydride material, making the material's measured capacities lower than would be obtained under quasi-equilibrium conditions.[5]

The capacities of the $LaNi_{5-x}Ge_x$ alloys are comparable to those of the $LaNi_{5-x}Sn_x$ alloys.[7,9,12,13] The x = 0.1 alloy had a moderate capacity in the first few cycles, until the viton O-ring seal is broken by pressure build-up in the cell. Although the x = 0.2 alloy has a plateau pressure greater than 1 atrn, it was able to achieve a reasonable electrochemical capacity, which attests to our cells being able to hold pressures slightly higher than 1 atm. However, its maximum capacity is still lower than the x'; 0.3 alloy, implying that either some of its storage capacity is not accessible or that the charge

efficiency of this alloy requires a charge return greater than 11 5%. The discharge capacity reaches a maximum near a Ge content of 0.3, unlike the Sri-substituted alloys which exhibit a peak in the capacity around x_{Sn} = 0.25. It was found from the gas-phase isotherm measurements that the absorption plateau pressure falls below 1 atm at a Ge composition ofx20.3,13 whereas the corresponding value for Sri-substituted alloys is x_{Sn} = 0.15.9 The maximum discharge capacity of Ge-modified alloys is almost 300 mAh/g, which is a respectable value for an AB_5 alloy under these conditions. In addition to the improvement in chargeability of the metal hydride electrode by reduced (absorption) plateau pressures, the use of Ge-substituted metal hydride anodes will result in Ni-MH cells of low operating pressures and low self-discharge.

ELECTROCHEMICAL KINETICS OF HYDROGEN ABSORPTION AND RESORPTION

The kinetics of hydrogen absorption and resorption are often slowed by the alloy substituents. This has been attributed to their tendency to form surface films that may alter the kinetics of charge transfer or hydrogen transport.[19] Tin substitutions, however, facilitate the hydriding kinetics at low solute concentrations, impeding the kinetics only at high concentrations? To quantify the effects of Ge substitutions on the kinetics, DC polarization and AC impedance experiments *were performed* on $LaNi_{5-x}Ge_x$ alloys in the charged condition. Micropolarization and Tafel measurements were performed on the alloys under potentiodynamic conditions at scan rates of 0.02 mV/s and 0.5 mV/s,

respectively. The scan rates were so chosen to provide near-steady state conditions with minimal changes in the state of charge of the electrode or its surface conditions,

Figure 4 shows the micropolarization curves of $LaNi_{5-x}Ge_x$ alloys. These curves are approximately linear. The exchange currents estimated from the slopes of micropolarization curves show an improvement in the kinetics of hydrogen absorption and resorption upon Ge substitution (Fig. 5 and Table 1). There is a small decrease at low Ge concentrations compared to the binary alloy, i.e., from 0.77 mA for the binary alloy to 0.63 and 0.71 for Ge compositions of 0.1 and 0.2, respectively. At higher Ge compositions, i.e.,x20.3, the exchange current is higher than that of the binary alloy and continues to increase with Ge content, Unlike the case for Sn solutes, which cause marginal slowing of kinetics at $x \geq 0.4$, high Ge concentrations have no adverse effects on the kinetics of hydrogen absorption.

To determine the kinetics of the absorption and resorption processes independently, Tafel polarization measurements were made on the $LaNi_{5-x}Ge_x$ alloys in the charged condition, For these Tafel polarization measurements, the electrode potential was scanned from extreme anodic values to the cathodic values, to avoid any uncertainties arising from hydrogen evolution on the alloy surface and the interference of gas bubbles adhering to the surface of the MH electrode. Fig. 6 illustrates the Tafel behavior of $LaNi_{5-x}Ge_x$ alloys during charge and discharge. As observed in our earlier studies, the Tafel polarization curves exhibit features similar to mass transfer-controlled processes. In

other words, the current tends to attain a limiting value at higher polarizations, a result of the diffusion-limited kinetics of hydrogen absorption and resorption. The limiting process could be a solid state diffusion of hydrogen in the MH alloys, which is relatively slower than the charge transfer process. The Tafel polarization data were corrected for the above mass-transfer interference by using the limiting currents. The limiting currents were measured in a separate potentiodynamic experiment at higher positive potentials, i.e., 400 mV away from the reversible potential, and are listed in Table 1. 'l'he diffusion limiting current on discharge is highest for a Ge composition of $0.1 < x \leq 0.2$ (in the range of 500 mA/g) and is reduced at high Ge compositions. The limiting currents appear to be symmetric for both the hydriding and dehydriding processes, and only desorption limiting currents are used to correct for the mass transfer interference. This is in contrast to the approach of Zheng, et al.[20] who used different limiting currents for charge and discharge. The latter approach might introduce uncertainties in the cathodic limiting currents, due to simultaneous hydrogen evolution at high negative potentials.[4]

Using the measured limiting currents, the Tafel plots can be corrected for the mass transfer effects by plotting the logarithm of $1/(1 - I/I_{lim})$ against the electrode potential. The exchange current density and transfer coefficients for hydrogen absorption were calculated from the intercept and inverse slope of the corrected cathodic Tafel plots, respectively. The corresponding coefficients for hydrogen resorption were calculated from the corrected anodic Tafel plots. The absorption exchange current density increases upon Ge

substitution and shows a maximum at a Ge composition of x = 0.3 (Fig. 7 and Table 1). The resorption exchange current improves more significantly upon Ge substitution, and also has a maximum near x = 0.3. Ge substitution improves the kinetics of both the absorption and resorption processes over the kinetics of the binary alloy. While Sn-substituted alloys show a maximum in the exchange current at very low compositions (x_{Sn} = 0.1 or 0.2), Ge -substituted alloys continue to have facile kinetics at higher compositions. Even after the maximum exchange current is reached, Ge-substituted alloys have faster kinetics than the binary alloy and Sri-substituted alloys with the same solute composition

The transfer coefficients from the Tafel data exhibit a trend consistent with that found with Sn substitutions. The transfer coefficient for the absorption process generally increases upon Ge substitution and is highest for x = 0.2, wherein the transfer coefficient for the resorption process decreases upon Ge substitution and increases only at high Ge concentrations, i.e., x== 0.5 (Table 1). As pointed out earlier, the plateau pressures for the absorption and resorption processes decrease with increasing Ge content. It is known[4] that lower plateau pressures facilitate absorption, whereas higher plateau pressures are desirable for resorption. The transfer coefficients calculated from the cathodic Tafel slopes (Fig. 8 and Table 1) range from 0.24 for the binary alloy to 0.39, 0.4, 0.35, 0.27 and 0.35 for x values of 0.1, 0.2, 0.3, 0.4 and 0.5, respectively. The

cone spending transfer coefficients during desorption are 0.55 for x = O, and 0.61, 0.35, 0.31,0.32 and 0.47 for x values of 0.1,0 .2,0.3,0.4 and 0.5, respectively.

Electrochemical Impedance Spectroscopy (EIS) measurements were also made on the $LaNi_{5-x}Ge_x$ MH alloys. The EIS data were obtained in the frequency range of 100 kHz to 5 mHz at a low AC amplitude of 2 mV. The impedance plots of $LaNi_{5-x}Ge_x$ alloy electrodes are shown in the Nyquist or Cole-Cole form in Fig. 9. The figure shows that the impedance increases slightly upon initial substitution of Ge, but decreases for $x \geq 0.3$. The impedance data were analyzed using a generalized equivalent circuit adopted for the MH electrode.[21] The observed impedance patterns of the MH electrodes are simplified by the absence of a diffusional component. The parameters in the equivalent circuit were calculated by a non-lines least squares fit using the Boukamp method .22 The. exchange current calculated from the charge transfer resistance decreases initially upon the substitution of Ge but increases for Ge compositions $x \geq 0.3$ (Fig. 5 and Table 1). This trend is similar to that observed in the DC polarization experiments.

It is thus clear that the electrochemical kinetics of hydrogen absorption and resorption improve markedly upon Ge substitution, as also observed with Sn substitutions. Unlike $LaNi_{5-x}Sn_x$ alloys however, the kinetics of $LaNi_{5-x}Ge_x$ alloys do not seem to be suppressed at high solute concentrations. Instead, the kinetics appear to be more facile in alloys with high Ge concentrations. The transfer coefficients of the $x = 0.5$ alloy are not consistent with this trend, perhaps because of its two-phase nature. This

will help simplify the optimization of Ge content in the alloy, since high Ge concentrations were also found to be beneficial for cycle life.

CYCLE LIFE

The capacity retention of $LaNi_{5-x}Ge_x$ alloys was measured during charge/discharge cycling in 300 mAh, negative-limited laboratory test cells. The cells were charged at a C/5 rate (60 mA/g) with a charge return of 115'%0 and discharged at C/2 (150 mA/g) to -0.5 V vs. Hg/HgO. The open circuit stand times between charge and discharge were set to 15 min. The time between discharge and subsequent charge is important because of the enhanced corrosion of the Ml-1 alloy in the discharged state.[23] Fig. 10 shows the capacity of the cells containing $LaNi_{5-x}Ge_x$ alloys with $0.1 \leq x \leq 0.5$ during 500 electrochemical cycles.

The capacity loss rate of the $LaNi_{5-x}Ge_x$ alloys is rather unusual. There is an initial, rapid drop of 5 - 20% in the capacity of all the alloys in the first 20 cycles, followed by an exponential decay. The mechanism underlying this rapid initial fall is not clear yet. Studies are underway to determine whether it is related to any noticeable morphological change such as particle size reduction, or a change in chemical order or composition, Even with this rapid initial fall, the capacity retention of the $LaNi_{5-x}Ge_x$ alloys during long term cycling is impressive compared to the binary or Sn-substituted alloys. After 400 deep (100%) discharge cycles, the capacities are still in the range of' 125

and 150 mAh/g for alloys with Ge compositions of 0.4 and 0.5, respectively. The capacity retention of the alloys containing Ge in the range of 0.4 - 0.5 is almost comparable to that of the commerical $MmNi_{3.5}Co_{0.8}Mn_{0.4}Al_{0.3}$, although the capacity in the initial stages is lower.

The cycle life curves are exponential in nature implying that degradation takes place as a first order reaction with the amount of degraded material proportional to the amount of active material. After the powders have undergone complete activation, the curves can be fit to an exponential decay, as done by Willems et al,[5] as:

$$C(n) = C_0 \; e^{-\delta n}$$

where C(n) is the capacity after n charge-discharge cycles, Co is the initial capacity, and the parameter δ denotes the exponential decay rate parameter. Fig. 11 shows the dependence of the capacity degradation rate on solute concentration in both $LaNi_{5-x}Ge_x$ and $LaNi_{5-x}Sn_x$ alloys. The figure shows that the rate of capacity loss during electrochemical cycling decreases linearly with increasing solute concentration. Furthermore, the capacity degradation constant is lower for Ge-substituted alloys than for Sri-substituted alloys. The corresponding characteristic degradation constant for a commercial $Mm(Ni\ Co\ Mn\ Al)_5$ alloy from Rhone-Poulenc, Inc. is around 0.0022, which could be achieved with solute compositions of $x_{Ge} = 0.40$ or $x_{Sn} = 0.42$. In other words,

the capacity retention made possible with a simultaneous substitution of several elements such as Co, Mn, and Al in misch metal based alloys can be realized with Ge alone. This could have significant implications on the processing cost and recycling of Ni-M H rechargeable cells, two important considerations for their widespread use. Although the price of Ge is high, Ge is an abundant element in the earth's crust. Much of the price of Ge originates with the need to refine it to electronic grades of purity.

CONCLUSIONS

We carried out a detailed electrochemical evaluation of $LaNi_{5-x}Ge_x$, where $0.0 \leq x \leq 0.5$. These alloys have the Haucke phase ($CaCu_5$) crystal structure and are single-phase for $x < 0.5$. The plateau pressures for the hydrogen absorption and resorption processes decrease with increasing Ge content. Alloys with $x_{Ge} \geq 0.2$ have plateau pressures suitable for charging in partially scaled cells, and have electrochemical capacities of approximately 290 mAh/g. The $LaNi_{5-x}Ge_x$ alloys show compositional trends for hydrogen absorption similar to those of $LaNi_{5-x}Sn_x$, although more Ge than Sn is needed to attain the same plateau pressure. The kinetics of hydrogen absorption and desorption improve upon Ge substitution. Unlike Sri-substituted alloys which show slightly suppressed kinetics at high Sn content, the kinetics of Ge-substituted alloys are improved at high Ge contents. The capacity retention of Ge-substituted alloys during

the capacity retention made possible with a simultaneous substitution of several elements such as Co, Mn, and Al in misch metal based alloys can be realized with Ge alone. This could have significant implications on the processing cost and recycling of Ni-MH rechargeable cells, two important considerations for their widespread use. Although the price of Ge is high, Ge is an abundant element in the earth's crust. Much of the price of Ge originates with the need to refine it to electronic grades of purity.

CONCLUSIONS

We carried out a detailed electrochemical evaluation of $LaNi_{5-x}Ge_x$, where $0.0 \leq x \leq 0.5$. These alloys have the Haucke phase ($CaCu_5$) crystal structure and are single-phase for $x < 0.5$. The plateau pressures for the hydrogen absorption and resorption processes decrease with increasing Ge content. Alloys with $x_{Ge} \geq 0.2$ have plateau pressures suitable for charging in partially sealed cells, and have electrochemical capacities of approximately 290 mAh/g. The $LaNi_{5-x}Ge_x$ alloys show compositional trends for hydrogen absorption similar to those of $LaNi_{5-x}Sn_x$, although more Ge than Sn is needed to attain the same plateau pressure. The kinetics of hydrogen absorption and desorption improve upon Ge substitution. Unlike Sri-substituted alloys which show slightly suppressed kinetics at high Sn content, the kinetics of Ge-substituted alloys ate improved at high Ge contents. The capacity retention of Ge-substituted alloys during

4. "I'. Sakai, M. Matsuoka, and C. Iwakura, in *Handbook on the Physics and Chemistry of Rare Earths,* K. A. Gschneidner, Jr. and L. Eyring, eds., Vol. 21, Elsevier Science B. V., Amsterdam (1995), p. 133.

5. J. J. Willems, *Philips J. Res.* **39 (Suppl. 1),** 1 (1984); J. J. Willems and K. H. J. Buschow, J. *Less-Common Met.*, 129,13 (1 987).

6. R. C. Bowman , Jr., C. H. Luo, C. C. Ahn, C. K. Witham and B. Fultz, *J. Alloys Comp.*, 217, 185 (1995).

7. B.V. Ratnakumar, G. Halpert, C. Witham and B. Fultz, *This Journal,* 141, 1.89 (1994); B. V. Ratnakumar, C. Witham, R. C. Bowman, Jr., A. Hightower, and B. Fultz, *This Journal, 143,2578* (1996).

8. S.W. Lambert, D. Chandra, W.N. Cathey, F.E. Lynch, and R.C. Bowman, Jr., *J. Alloys Comp.*, 187,113 (1992)

9. S. Luo, W. Luo, J. D. Clewley, T. B. Flanagan and L. A. Wade, *J. Alloys Comp.*, 231,467 (1995)

10. F. Meli, A. Züttel, and L. Schlapbach, *J. Alloys Comp.*, 190, 17 (1992); F. Meli, A. Züttel, and L. Schlapbach, *Zeitschrift für Physikalische Chemie, 1.83,371 (1994).*

11. F. Meli and L. Schlapbach, *J. Less-Common Met.*, 172-174,1252 (1991).

12. C Witham, B.V. Ratnakumar, R. C. Bowman, Jr., A. Hightower, and B. Fultz, *This Journal., 143 (9), 1.205-1,208 (1 996).*

13. C. Witham, R. C. Bowman, Jr., and B. Fultz, *J. Alloys Comp.* (in press).

14. E. T. Teatum, K. A, Gschneidner, Jr., J. T. Waber, *Los Alamos Report # 4003*, (1968).

15. C. Jordy, A. Percheron-Guegan, J. Bouet, P. Sanchez, C. Chanson and J. Leonardi, J. *Less-Common Met.*, 172-174, 1236(1991).

16, For example, A. Anani and R.A. Huggins, *J. Power* Sources, 38,363 (1 992).

17. D. N. Gruen, M. H. Mendelsohn and A. E. Dwight, *J. Less-Common Met.*, 63, 193 (1979).

18, A. H. Boonstra, 1. N. M. Bernards, and G. J. M. Lippits, *J. Less-Cornmon Met.*, 159,327 (1990).

19. T. Sakai, H. Miyamura, N. Kuriyama, A. Kato and K. Oguru J. *Less Common Metals*, 159,127 (1990).

20. G Zheng, B.N. Popov, and R.E. White, *This Journal.*, **143** (3), 834 (1996).

21. N. Kuriyama, T. Sakai, H. Miyamura, I. Uehara and H. Ishikawa, *J. Alloys Comp.*, 192, 161 (1993).

22. B.A. Boukamp, Solid State Ionics, 20,31 (1986).

23. B.V. Ratnakumar, S. Surampudi, C. Witham, A. Hightower, R.C. Bowman, Jr., and El. Fultz, in *Proc. 37th Power Sources Conf.*, Cherry Ilill,NJ(1996), pp. 440-445.

FIGURE CAPTIONS

Fig. 1: p-c isotherms of $LaNi_{5-x}Ge_x$ alloys: (a) Gas-phase and (b) Electrochemical (Δ,▲ x== 0.5; □,■ x = 0.4; ○,● x = 0.3; ◊,♦ x= 0.2; , x== 0.1; open - charge, filled - discharge).

Fig. 2: Variation of mid-point discharge potentials (open, dashed) and the corresponding reversible potentials (filled, solid) calculated from the resorption plateau pressures, of $LaNi_{5-x}Ge_x$ (●) and $LaNi_{5-x}Sn_x$ (A) alloys.

Fig. 3: Maximum hydrogen absorption capacity of $LaNi_{5-x}Ge_x$ (.) and $LaNi_{5-x}Sn_x$ (▲) alloys measured with Sievert's apparatus (filled), and prismatic cel 1 electrode (open).

Fig. 4: Linear polarization curves of $LaNi_{5-x}Ge_x$ alloys,

Fig. 5: Variation of the exchange current density from measurements by DC micropolarization (open, dashed) and AC Impedance (filled, solid) of $LaNi_{5-x}Ge_x$ (●) and $LaNi_{5-x}Sn_x$ (A) al loys.

Fig. 6: Tafel polarization curves without mass transfer corrections for $LaNi_{5-x}Ge_x$ alloys.

Fig. 7: Exchange current from Anodic (filled, solid) and Cathodic (open, dashed) Tafel Polarization data for $LaNi_{5-x}Ge_x$ (●) and $LaNi_{5-x}Sn_x$ (A) alloys.

Fig. 8: Transfer coefficients from Anodic (filled, solid) and Cathodic (open, dashed) Tafel Polarization data for $LaNi_{5-x}Ge_x$ (.) and $LaNi_{5-x}Sn_x$ (A) alloys.

Fig. 9: Electrochemical Impedance Spectroscopy (EIS) curves of $LaNi_{5-x}Ge_x$ alloys.

Fig. 10: Cycle life behavior of $LaNi_{5-x}Ge_x$ alloys with comparison to a good commercial misch-metal based, multi-component alloy also evaluated at JPI.

Fig. 11: Exponential decay parameter of $LaNi_{5-x}Ge_x$ (.) and $LaNi_{5-x}Sn_x$ (A) alloys for electrochemical cycling.

Table 1. Kinetic parameters of $LaNi_{5-x}Ge_x$ alloys determined by DC polarization and AC impedance methods

x in $LaNi_{5-x}Ge_x$	Micropoln.	Tafel Polarization				Desorp. Lim. Curr.	AC Impedance
		i_0, mA		Tafel Slope, mV/dec			
	i_0, mA	Absorp	Desorp	Absorp	Desorp	mA	i_0, mA
00	0.77	0.96	1.51	242	108	14	1.02
0.1	0.63	1.54	1.74	150	96	12	0.70
0.2	0.71	1.57	1.99	147	167	20	0.80
0.3	1.07	3.06	3.83	170	192	24	1.13
0.4	1.13	1.95	3.37	217	184	16	1.20
0.5	1.00	[illegible]	1.86	168	126	24	3.15

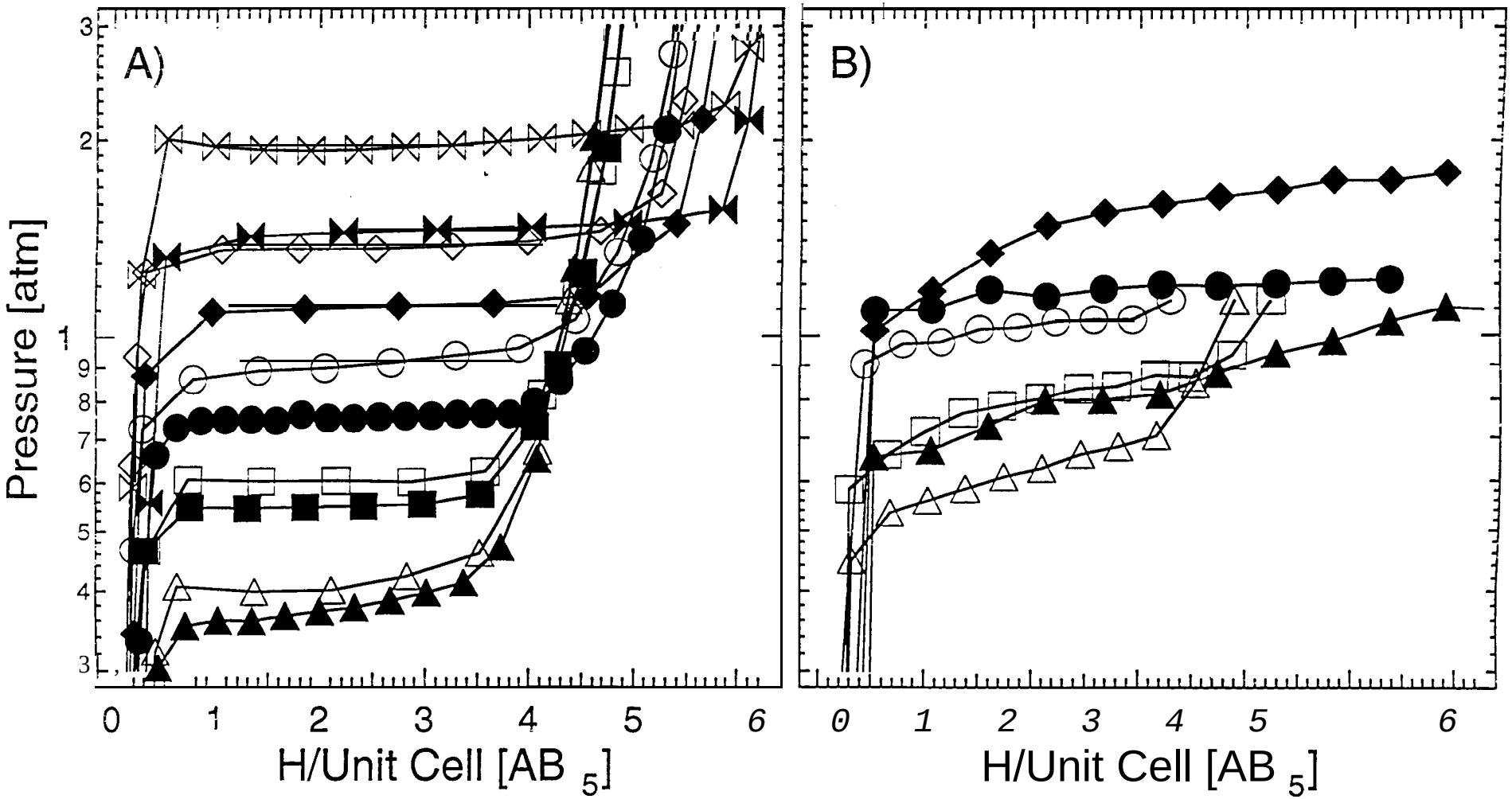

Please make this a 2 column figure

Witham, et al.

Figure 1

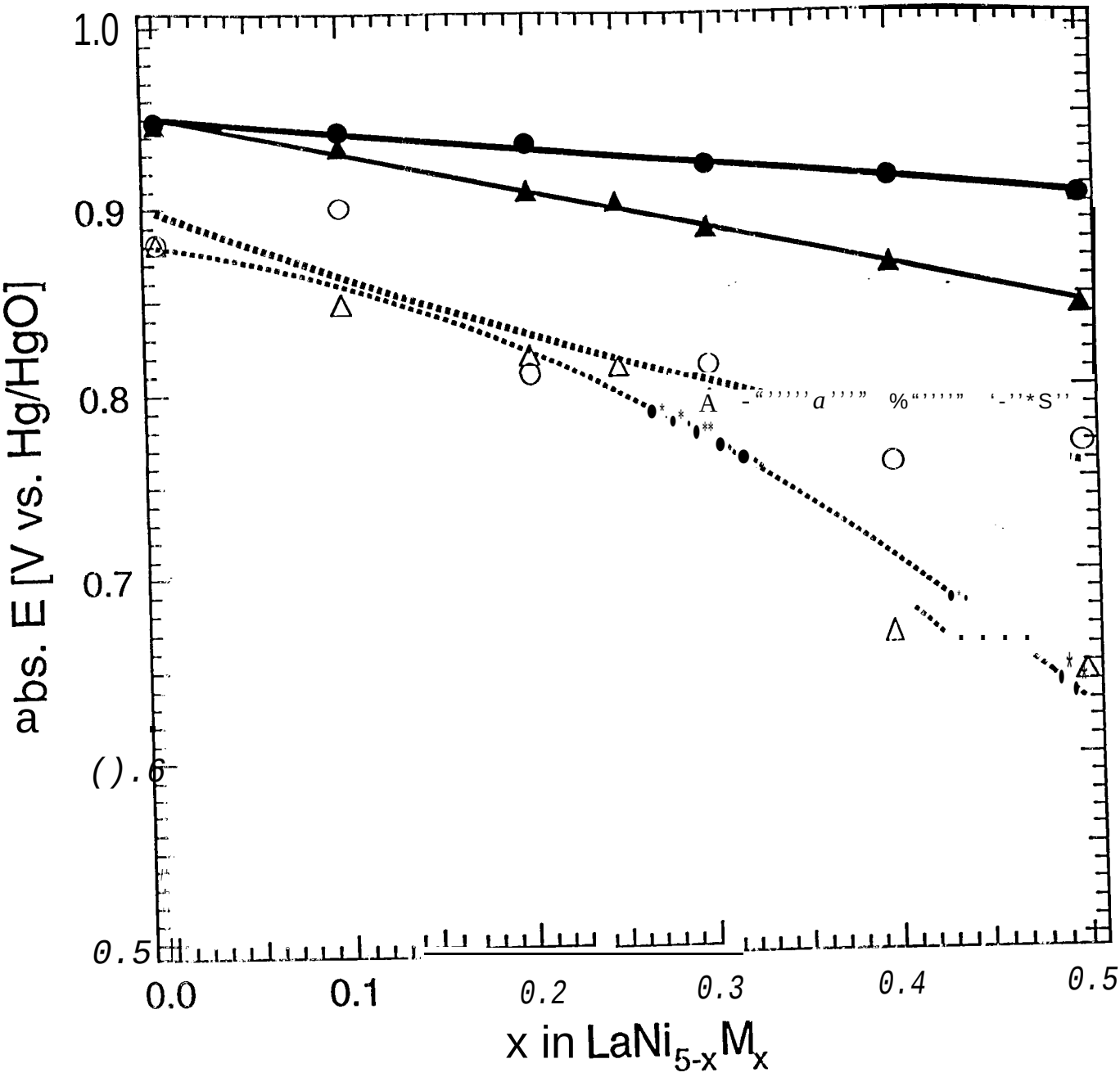

Witham, et al.

Figure 2

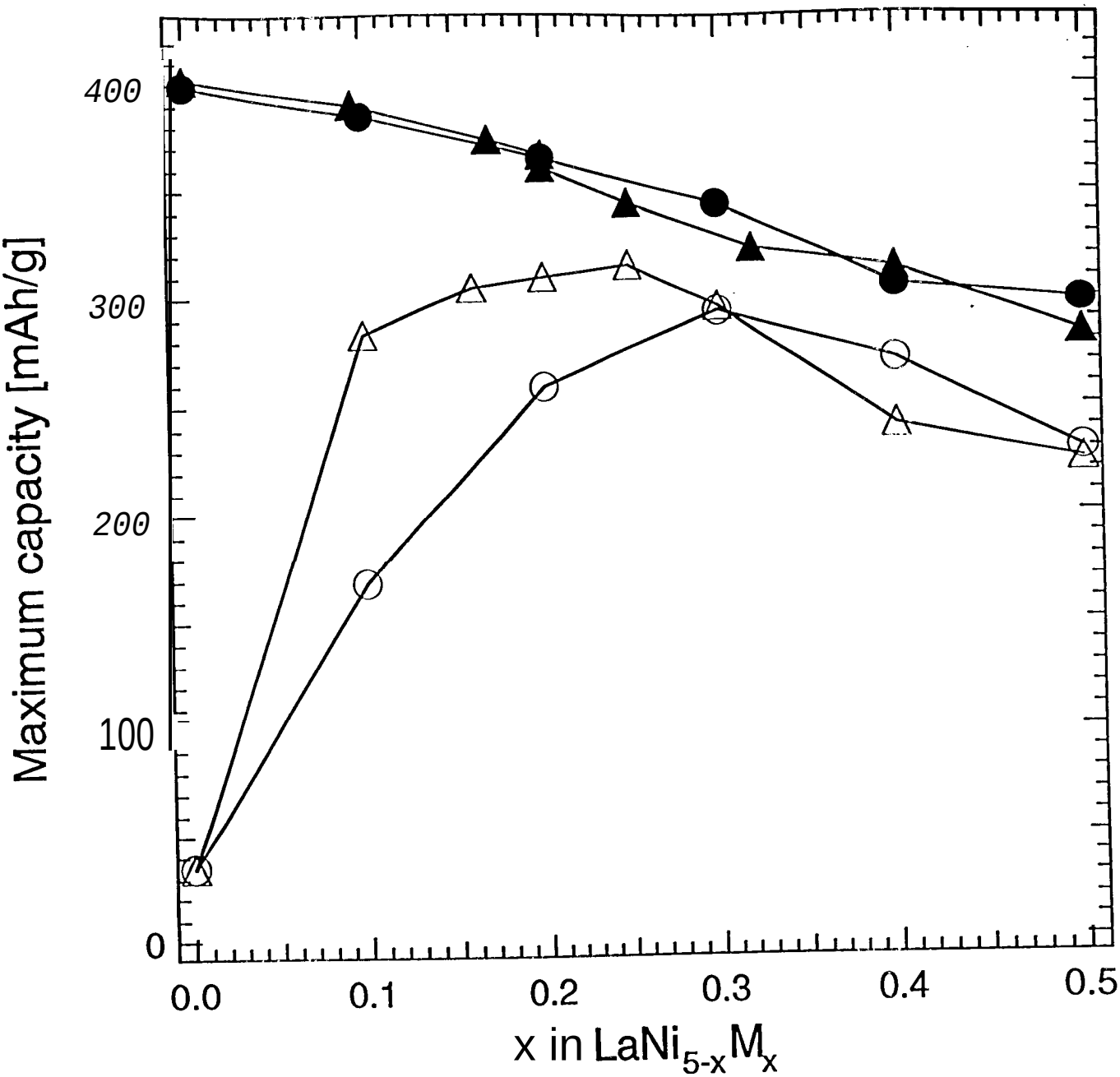

Witham, et al.

Figure 3

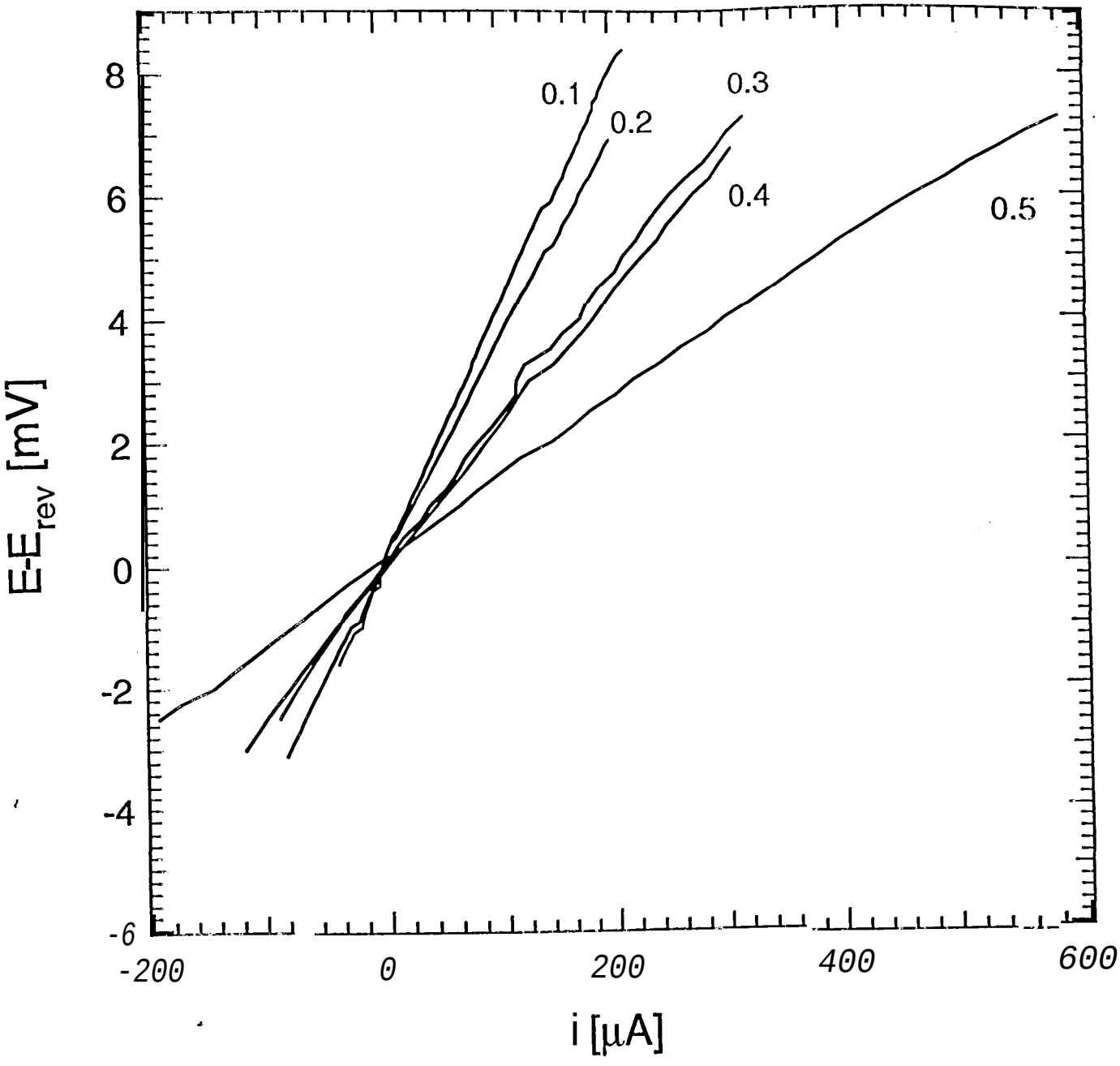

Witham, et al.

Figure 4

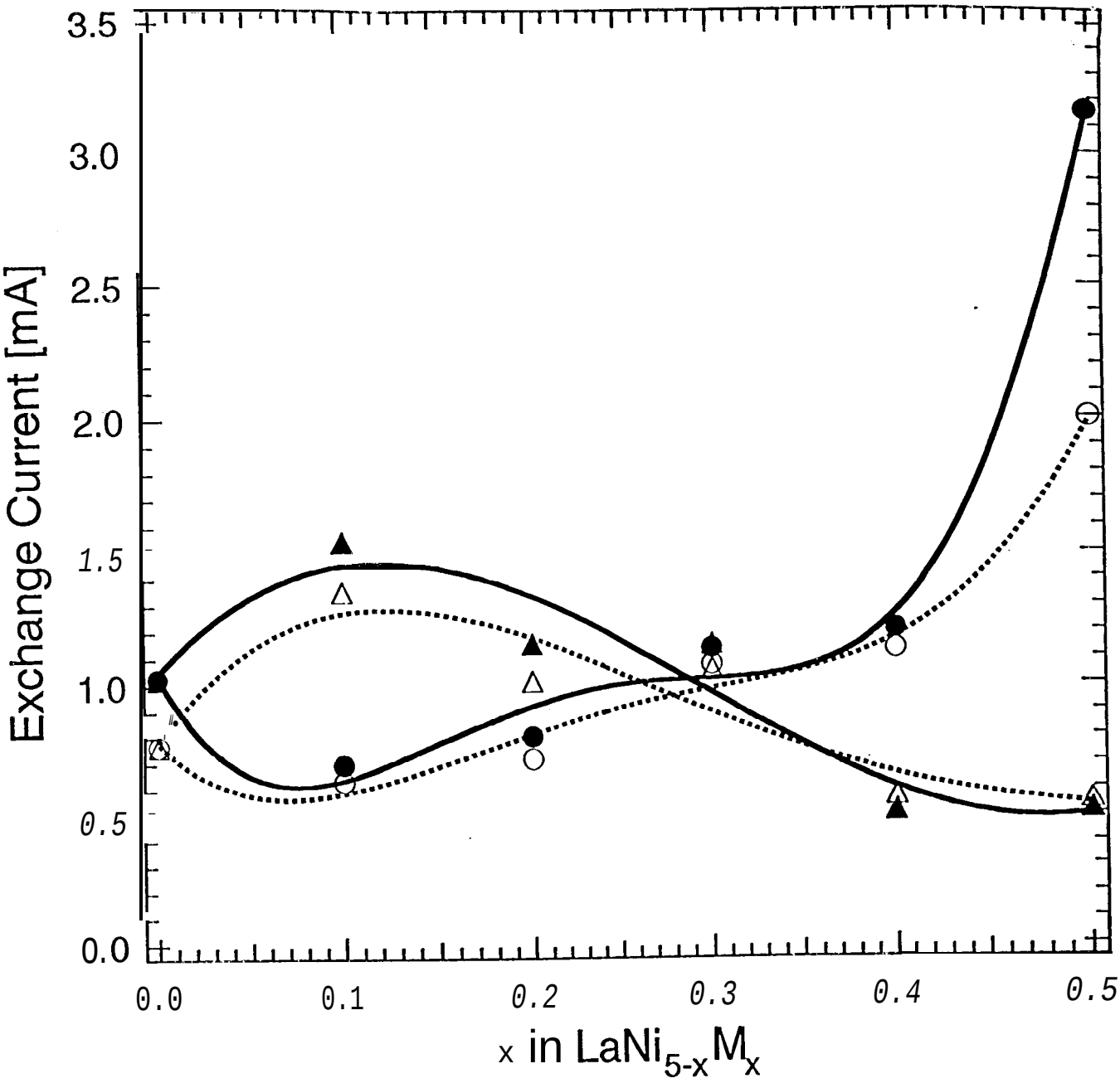

Witham, et al

Figure 5

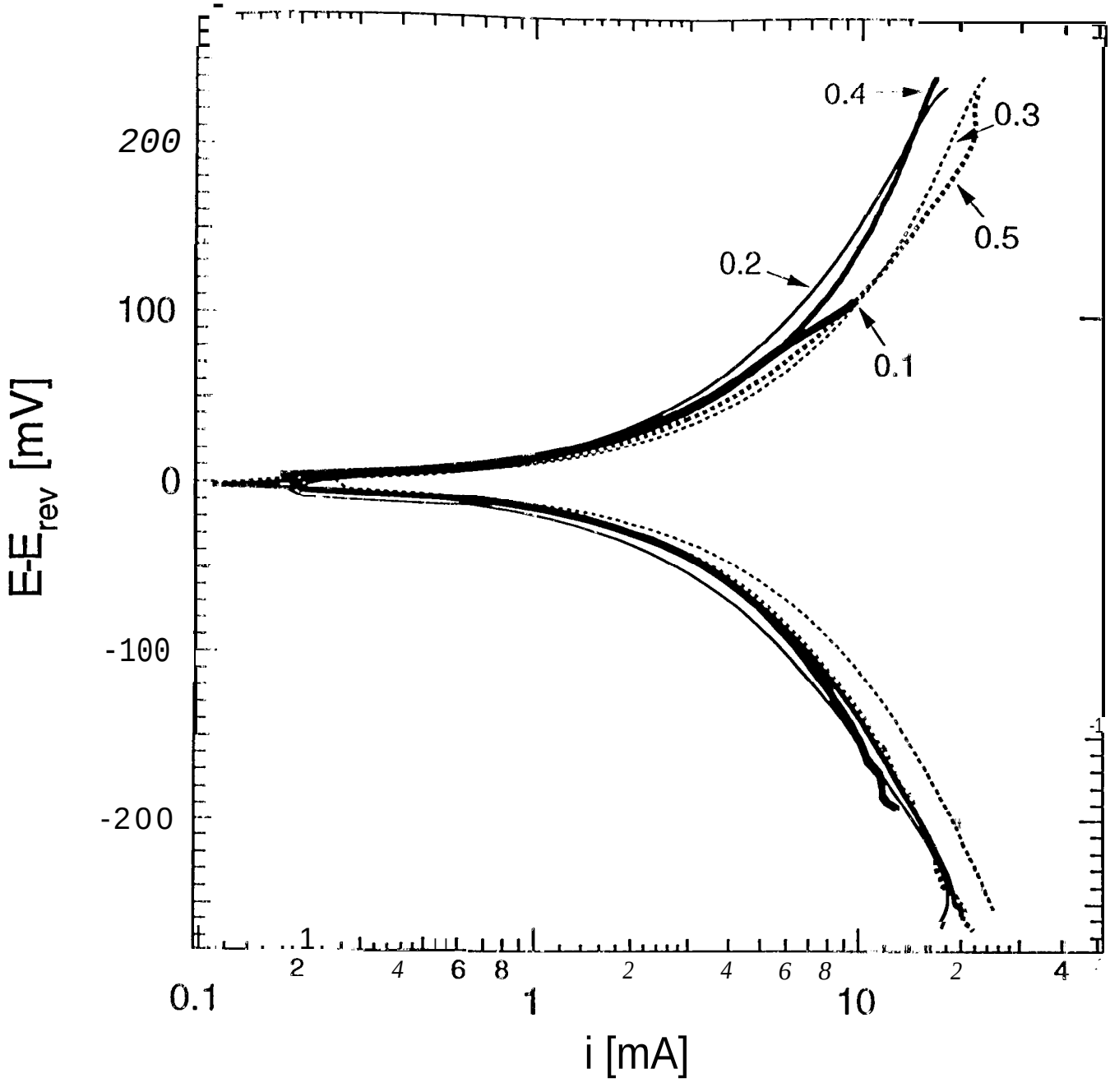

Witham, et al

Figure 6

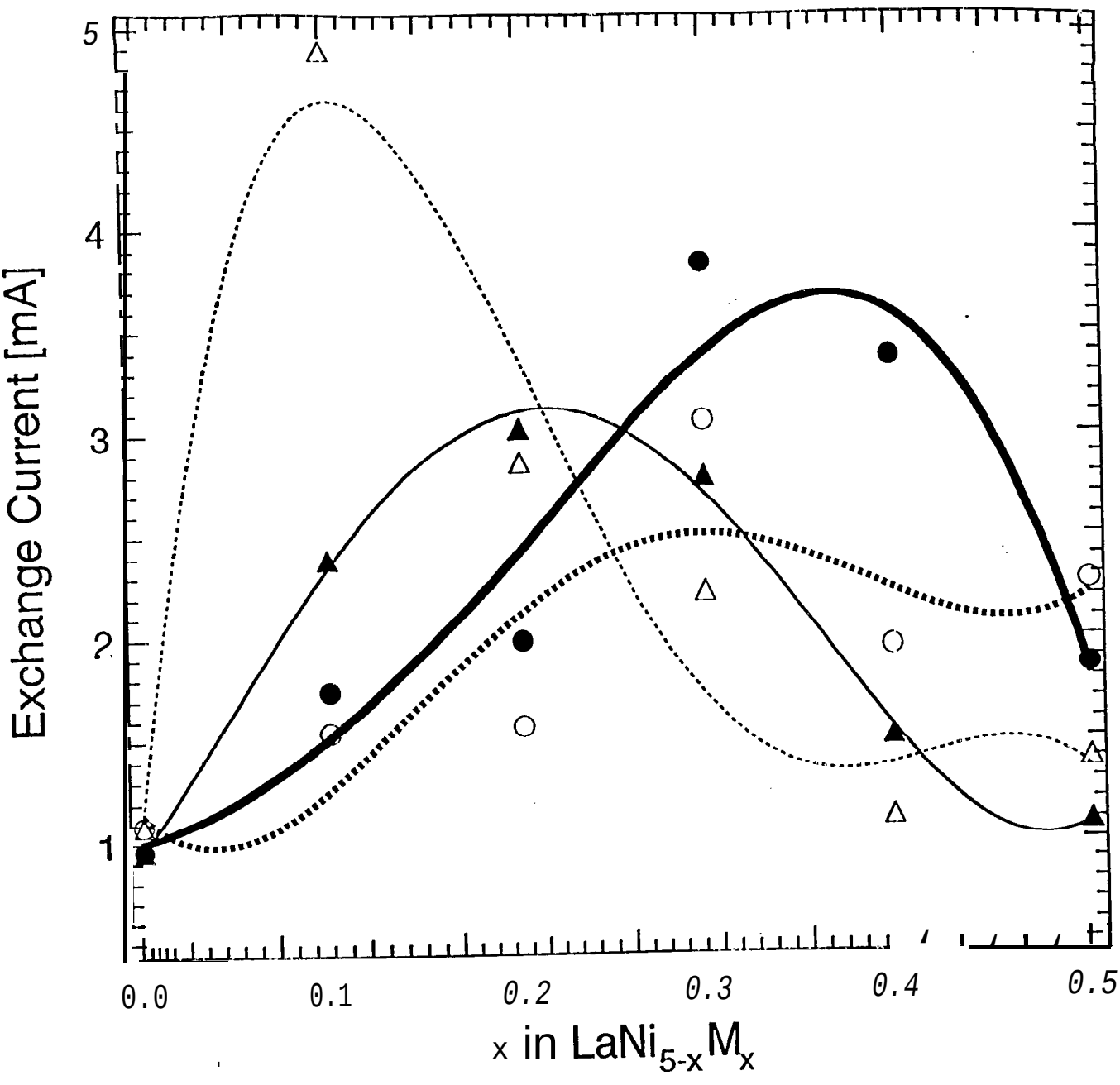

Witham, et al.

Figure 7

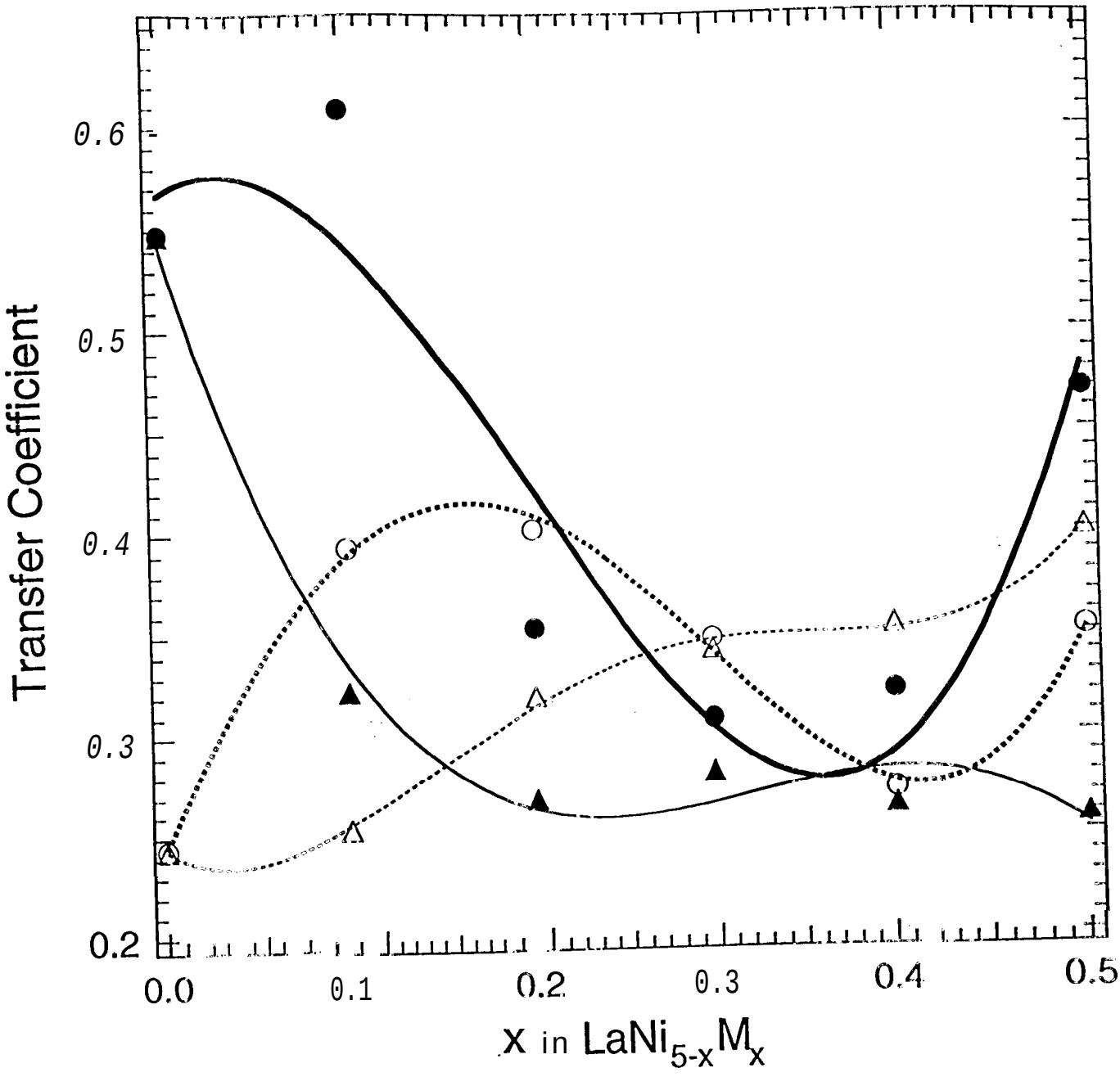

Witham, et al.

Figure 8

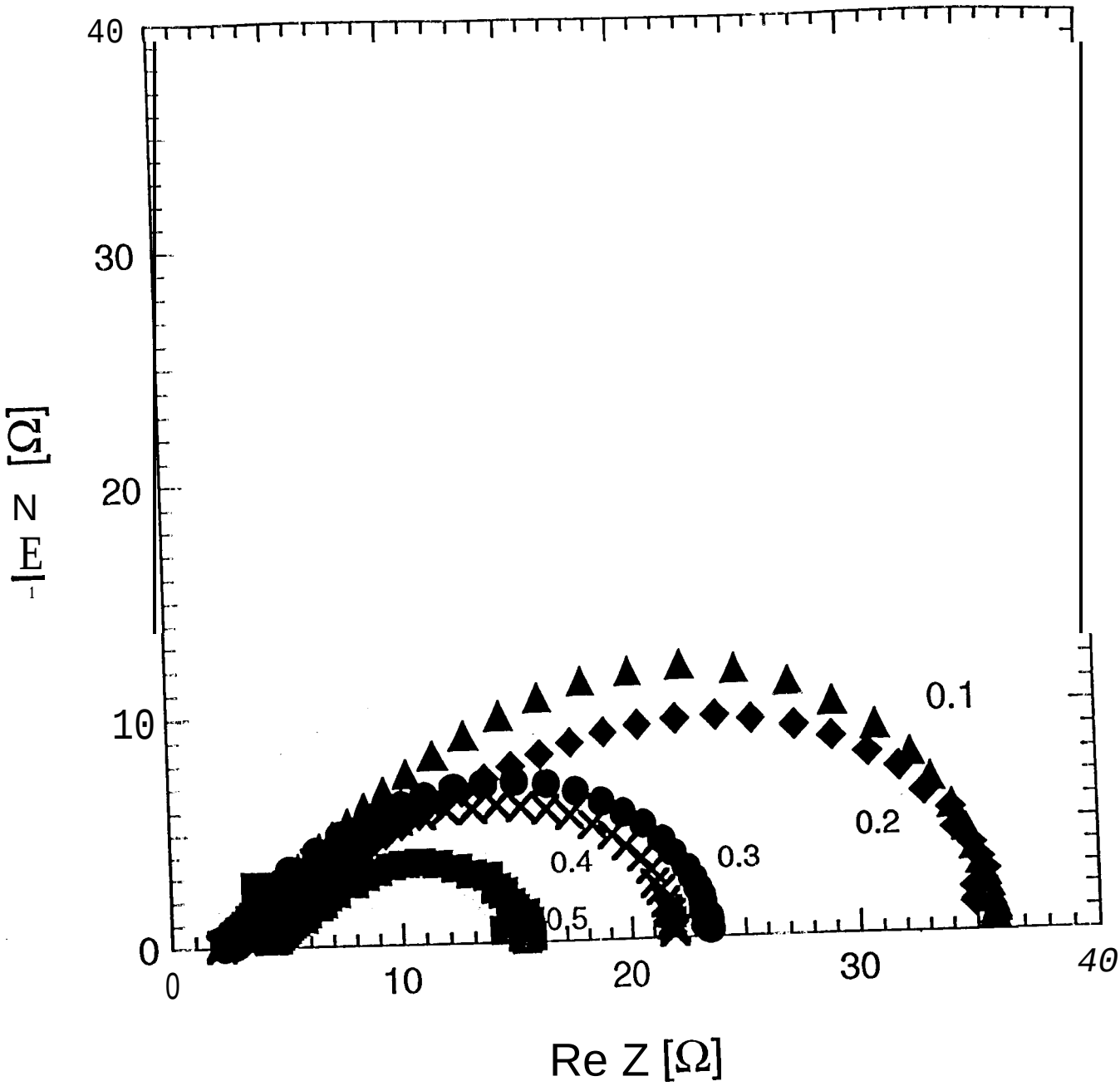

Witham, et al.

Figure 9

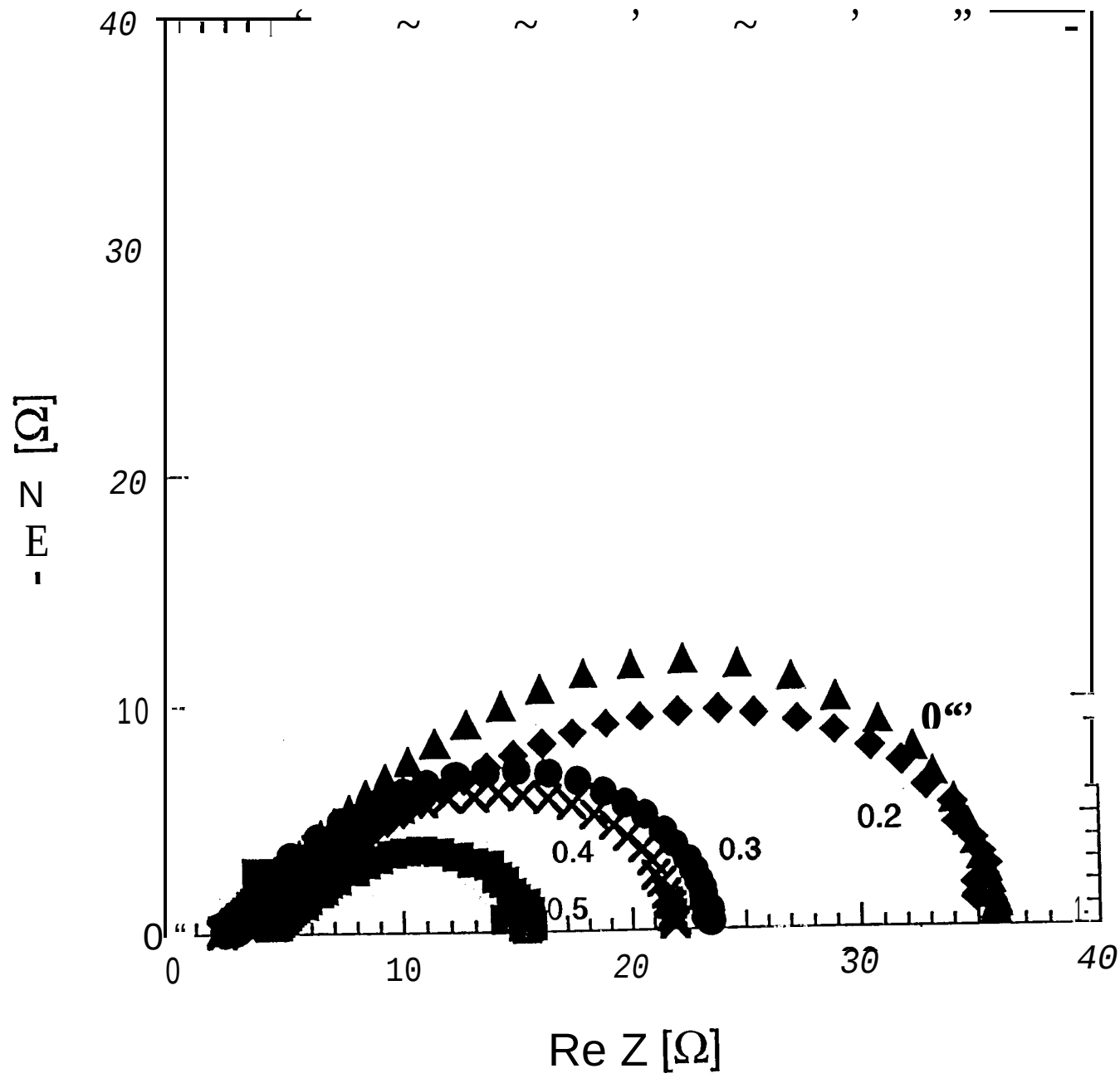

Witham, et al

Figure 9

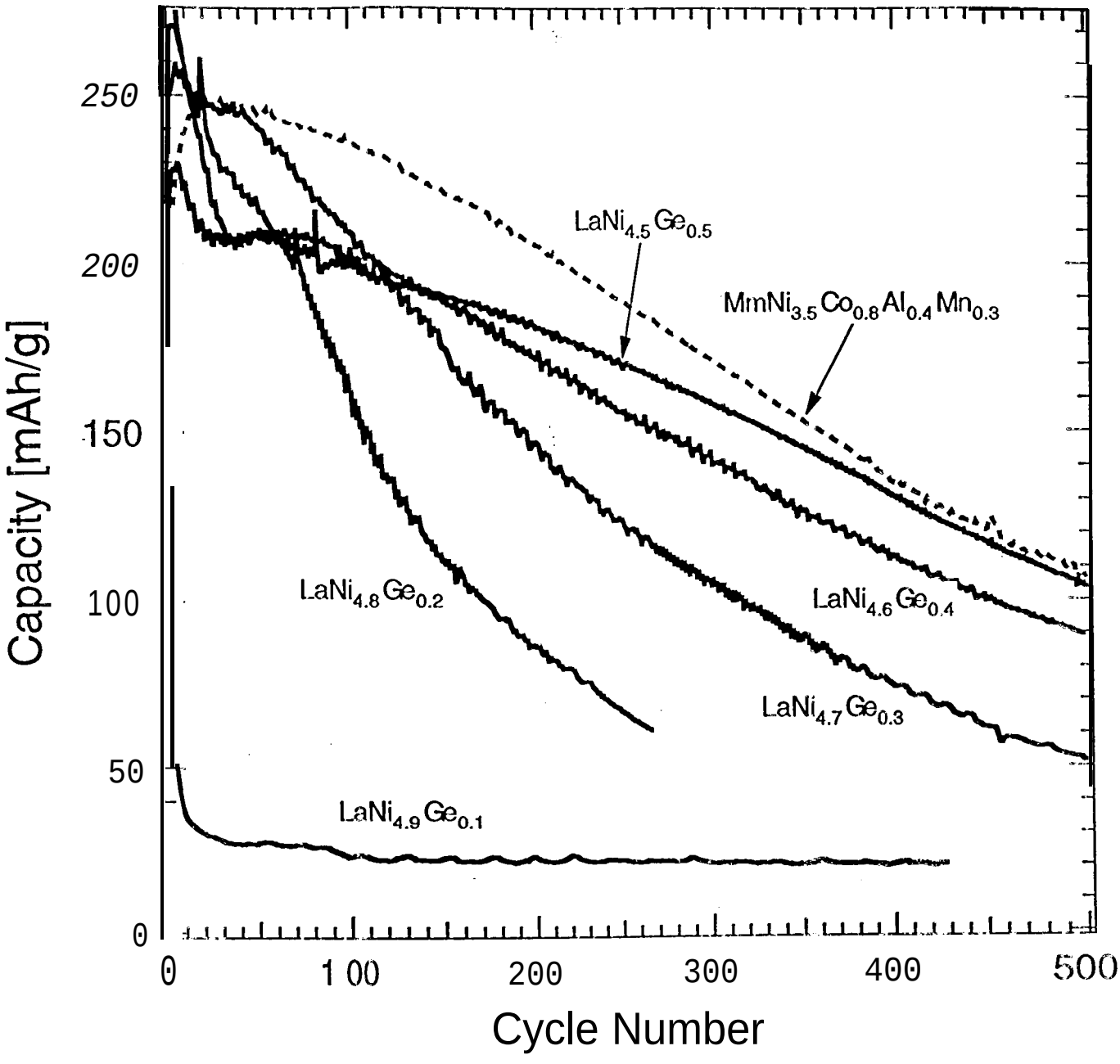
250
200
150
100
50
0
Capacity [mAh/g]
0
100
200
300
400
500
Cycle Number
LaNi4.5Ge0.5
MmNi3.5Co0.8Al0.4Mn0.3
LaNi4.8Ge0.2
LaNi4.6Ge0.4
LaNi4.7Ge0.3
LaNi4.9Ge0.1

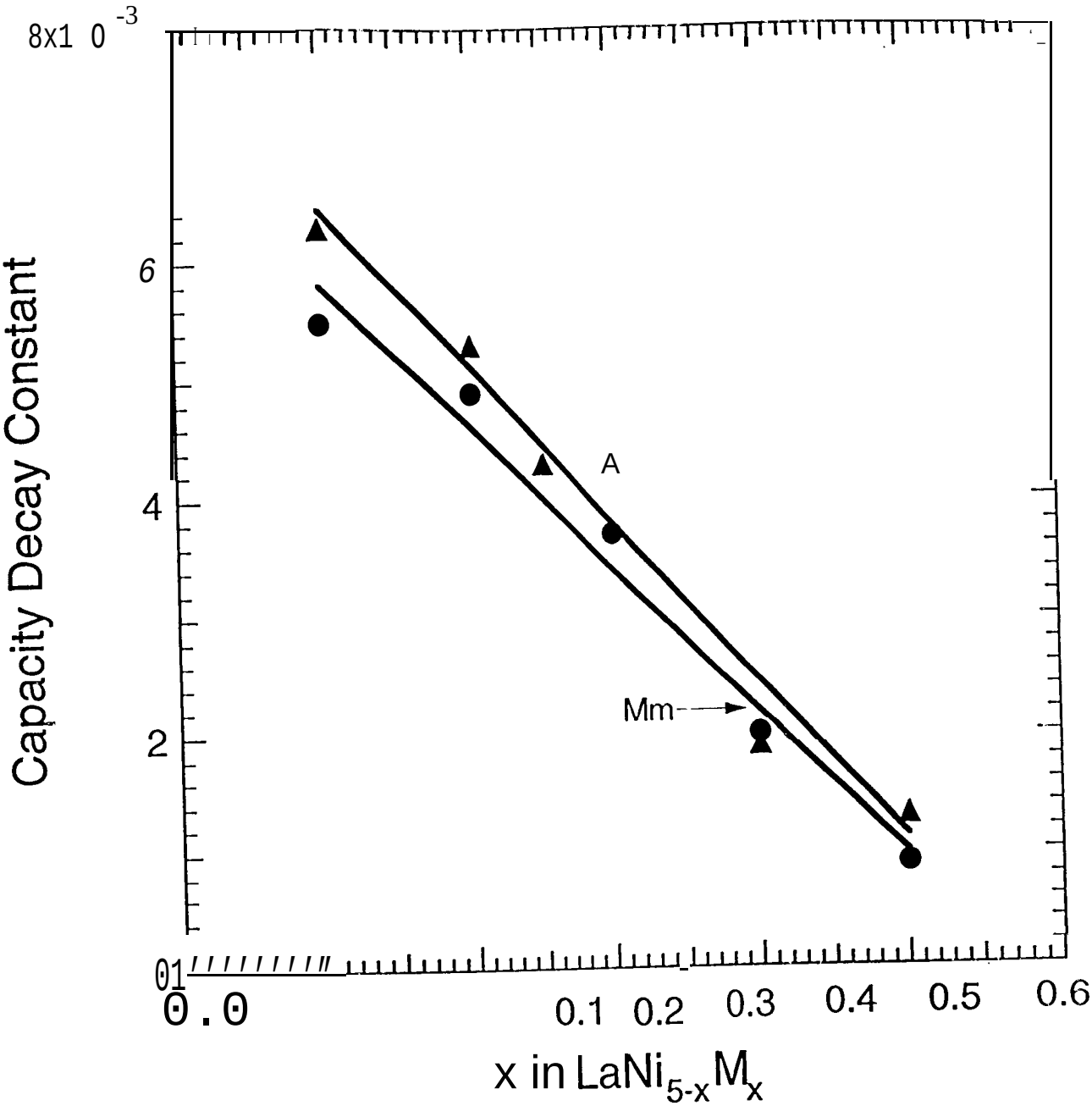

Witham, et al.

Figure 11